EU – FP7

AMARSi
Adaptive Modular Architectures for Rich Motor Skills

ICT-248311

D 1.4

April 2013 (36 months)

Report on segmentation of trajectories into the underlying primitives and syntactic rules for their compositionality based on differential geometry approaches

Prepared by Yaron Meirovitch[1] and Tamar Flash[1]

[1] Department of Computer Science and Applied Mathematics, Weizmann Institute of Science, Rehovot, Isreal.

Due date of deliverable	~~1 April 2013~~ 1 March 2013
Actual submission date	15 April 2013
Lead Partner	~~Santa Lucia Foundation~~ Weizmann Institute of Science
Revision	Final
Dissemination level	Public

Contents

Chapter 1

Introduction

A motor task can be represented by the degree of spatiotemporal accuracy needed to achieve a certain goal. For geometrically constrained motor tasks the goal is usually represented by a geometrical template (e.g. 'trace that ellipse') while more voluntary tasks usually involve the requirement to achieve a high level goal (e.g. 'cut the tomatoes'). The question how the nervous system is capable of generating complicated motion patterns by selecting among an enormous number of competing executions is an open question for all such motor tasks. One of the main goals of motor control research is to describe the repertoire of constrained and voluntary human movements in terms of basic elementary movements, i.e motion primitives (Bernstein (1967) and for a review see Flash and Hochner (2005)). Here we suggest a mathematical framework for geometric and kinematic descriptions of trajectories and algorithms for the segmentation of human task level trajectories. The described models were tested for path-constrained human drawing and locomotion trajectories.

The structure of the deliverable

In this deliverable we describe three motor control approaches to motor segmentation, kinematic representation and regularity extraction in highly noisy complex motor production. The underlying motivation is that geometry plays a central role in affecting and shaping the behavioral regularities in human end-effector movements.

The first study theoretically establishes the mathematical and computational tools for extracting differential affine properties from recorded data. Additionally, a relationship between the minimum jerk model and the mixed geometry model was proved for a special group of basic affine curves called affine orbits. An affine invariant segmentation of movements in task space is then suggested based on this family of orbits, subserving as candidate movement primitives. In future work we

intend to examine the robustness of this approach by studying whether such primitives consistently appear in repeated motor tasks, whether they are specific to individual performers and how well they generalize across geometrically related motor tasks. Additionally the minimum jerk profiles associated with the affine primitives will be studied and matched with human production kinematics.

In the second study we focus on the kinematic representation of human movement, complementing the purely geometric approach undertaken in the first study. The representation is based on the mixed geometry kinematic prediction (Bennequin et al. (2009)) which suggests a tensorial combination of velocity profiles based on the classical group transformations. We suggest here that adequate kinematic representation of drawing movements can be construed from specific control parameters at the critical points along the path, at which the geometry attains singularities. This descriptive study suggests a characterization of the kinematics by mixing geometries at the critical points and inferring the output profile by the interpolation of the mixtures along the entire path thus inferring the kinematics based on the use of the Euclidean and equi-affine curvatures.

In the third study we demonstrate how we can implement certain aspects of our approach in natural noisy and highly complex human trajectories recorded from the wrists movement of Israeli Sign Language (ISL) users. We demonstrate that equi-affine and other generalized power law regularities can be lawfully extracted from the recorded trajectories by assuming an underlying segment-wise polynomial time development of the end-effector's Cartesian trajectory. We employed a Bayesian Binning approach (Endres et al. (2008)) because the high time derivatives of position in the highly complex natural data are extremely noisy and no other previous work has attempted to uncover underlying power law segmentation by assuming a polynomial model. It appears that kinematic regularities can be reliably identified by Bayesian Binning and that the previously reported results relating minimum jerk to the generalized power laws by Richardson and Flash (2002) are valid also for the internal structure of those complex movement data.

Power Laws, Smoothness Maximization and Isochrony

In the following section we review several previous findings related to the approach described in this manuscript while focusing on the theoretical relationships between the different models and empirical findings.

Previous studies focused on the stereotyped kinematic output of human movements, known as human kinematic regularities. One important motor regularity representing the relationship between the path and kinematics followed by the end-effector is based on the empirical finding concerning the coupling between curvature and speed in different motor tasks. This relationship was described by the "Two Thirds Power Law" which expresses the observation that the movement speed is piecewise proportional to the radii of curvature raised to the one third. The robust properties of this law established it as a kinematic regularity in humans and in other primates and as a biomarker

of biological motion. Later, this empirical finding was mathematically expressed by using equi-affine geometry (Handzel and Flash (1996), and Pollick and Sapiro (1996)). Another observed regularity is the tendency of reaching movements to follow nearly straight hand paths with bell-shaped velocity profiles. Using a first principles approach, these empirical observations were accounted for based on the minimization of hand jerk (Flash and Hogan (1985); Richardson and Flash (2002)).

Another global regularity, reported in the literature, is related to the finding that durations of human movements sub-linearly depend on movement amplitudes, e.g. when two figural forms, differing only in their spatial scales are drawn they have roughly equal durations. This is called the isochrony principle (Viviani and McCollum (1983); Viviani and Flash (1995)). Related temporal regularities appear also within the production of goal directed movements, e.g. in obstacle avoidance or movements constrained to pass through a via-point movements where approximately half of the total duration is devoted to reaching the via-point even though the via point is not placed half way along the axis connecting the initial and final via points (Flash and Hogan (1985)). These related phenomena are thought to stem from a temporal regulation by which total timing is equally shared by different motor subtasks. These phenomena were collectively termed under one principle – Isochrony (Viviani and Flash (1995)).

A further work examining the relation between smoothness maximization (minimum jerk) and equi-affine geometry (and in particular, the two thirds power law) was represented in two papers by Polyakov and colleagues which identified different movement paths which obey both the minimum jerk model and the two-thirds power law (Polyakov et al. (2009a,b)). These studies found that equi-affine geodesics, parabolic paths, minimize hand jerk, obey the two-thirds power law and are invariant under affine transformations. Also, it was observed that affine transformations can be used to generate any parabolic stroke from an arbitrary parabolic template, and a few parabolic strokes may be concatenated to compactly form a complex path. To test the possibility that parabolic elements were used to generate planar movements, they analyzed monkeys' scribbling trajectories. Practiced scribbles were well approximated by long parabolic strokes. Of the motor cortical neurons recorded during scribbling more were related to equi-affine than to Euclidean speeds. Unsupervised segmentation of simultaneously recorded multiple neuron activities yielded states related to distinct parabolic elements (Polyakov et al. (2009a,b)).

Finally, Bennequin et al. (2009) presented a theory of movement generation based on movement invariance with respect to geometrical transformations, integrating several of the previous empirical findings, namely, the two thirds power law and the isochrony principle into one motor theory. Their study employs three classical transformation groups, Euclidean, equi-affine and full affine. Full affine transformations preserve only parallelisms of lines and their incidence whereas equi-affine transformations preserve also area. A further restriction is given by the Euclidean transformations which preserve also lengths and angles. According to their motor theory, movement timing is continuously prescribed by the brain by combining different "geometrical times" each assumed to be

proportional to the measure of distance of the corresponding geometry. Movements are constructed by using a series of instantaneous (Cartan) moving coordinate frames. The predictions of this theory were validated based on experimental observations of human drawing and walking. Three prominent motor behaviors are modulated by mixing among geometries, the equi-affine geometry (representing the 2/3 power law) the full-affine geometry (representing the isochrony principle) and the Euclidean geometry (representing constant speed movements). The three geometries were suggested to be combined either by segmenting the movement serially in time (inter-segment) or within the same segment by a tensorial operation (intra-segment multiplication). It was experimentally validated that modulating the movement by selecting each of the geometries for each segment was insufficient to account for the kinematic and temporal features of different motor tasks. However, the tensorial operation, which enabled a mixture of the geometries within a segment, was highly successful in explaining the data. For the tensorial combination they used exponent weights, which added degrees of freedom to the computational model. Furthermore, the tensorial operation enabled an identity in dimensions between time and space, selectively entailed by the particular mixture. For instance, executing movement based on a purely affine law yields profiles of Euclidean, equi-affine, and affine speeds. By an affine transformation of the movement, such as scaling of the spatial dimensions by a fixed factor and keeping the time dimension intact, the affine profile is unchanged (the Euclidean profile will be scaled by the factor and the equi-affine profile will be scaled by the factor raised to the power of two-thirds).

Chapter 2

The current geometrical approach for affine segmentation

The fact that earlier observations have shown that various movements are stereotypical (Lashley (1951), Bernstein (1967), Abend et al. (1982), Flash (1983), Flash and Hogan (1985), Harris and Wolpert (1998), Mussa-Ivaladi FA (2000), Bizzi et al. (2000), Flash and Hochner (2005)) has guided the study of motor organization which traditionally looked for unifying organizing principles. Here we are suggesting the use of a purely geometrical approach for defining a family of prototypical figural forms that can be used to represent and segment complex human end-effectors trajectories. The idea motivating this research is that different geometries unify empirical observations concerning human movement, specifically the two-thirds power law, the isochrony principle and the stereotypical maximally smoothed movements (Bennequin et al. (2009)).

Typical figural forms defined by Affine Orbits

In previous studies by Olver et al. (1994) and Calabi et al. (1998) it has proven useful to study the osculating fundamental curves of a given path. It was noted that the point-wise geometric properties of the target curve are captured by the respective properties of the osculating one. For example, when studying Euclidean invariants, one considers the fundamental Euclidean curves, which are circles and straight lines. In equi-affine geometry, the fundamental curves are parabolas, hyperbolas and ellipses (conic sections). Respectively to each of the mentioned geometries, these curves are the ones having constant curvatures and are the orbits of the corresponding transformation groups. The differential properties of an orbit that are defined by the geometry are always constant functions of the arc-length parameter and all points of the orbit are the same from the point of view of the

Geometry	Orbits	Differential Invariant
Euclidean	Circles, straight lines	Euclidean curvature
Equi-affine	Conic sections (ellipses, parabolas, hyperbolas)	Equi-affine curvature
Affine	Conic sections, monomials (parabolic, hyperbolic), log spirals, exp. curves, straight lines	Affine curvature

respective geometry; the Euclidean curvatures of circles and straight lines are constant functions of the Euclidean arc-length parameter and the equi-affine curvatures of the conic sections are constant functions of the equi-affine arc-length parameter. Therefore, in each of these geometries, studying the osculating orbits of a general path provides us with the invariants of the geometries.

To study the full affine invariants of a general curve, we must ask what are the fundamental curves of planar (full) affine geometry; we find that these are mainly the Lie group orbits generated by the 1-dimensional Lie algebras of 2-by-2 matrices (Guggenheimer (1977), Faugeras and Keriven (1996), Bennequin et al. (2009)),

$$G_A = \{A\varsigma | \varsigma \in \mathbb{R}\},$$

where $A \in \mathbb{R}^{2\times 2}$ is a fixed matrix. The resulting trajectory of the affine orbit, $r(\varsigma)$ is:

$$r(\varsigma) = \exp(A\varsigma)p_0.$$

Geometric Parameterization of Affine Orbits

In order to develop the framework relating the affine orbits and the Mixed Geometry model (Bennequin et al. (2009)) and the Minimum-Jerk model, we first calculated the Euclidean, equi-affine and affine parameterizations of the affine orbits. Based on the mixed geometry model, we defined a new parameter, z , that takes into account the tensor contributions of the three geometries, Euclidean, equi-affine and affine:

$$dz = C_2^{\beta_2} C_1^{\beta_1} C_0^{\beta_0} ds^{\beta_2} d\sigma_1^{\beta_1} d\sigma_0^{\beta_0} \tag{2.1}$$

where C_2, C_1, C_0 are the constant Euclidean, equi-affine and affine velocities, respectively.

Affine orbits, Mixed Geometry and Minimum-Jerk descriptions

The inspection of the affine orbits was initiated in our research in order to derive the affine curvature of a general curve. Although methods for doing so existed based on analytic expressions, the

Geometry	Orbit Parametrization
Equi-Affine	$\varsigma = \frac{3}{traceA} \ln\left(\frac{trace(A)}{3}\left\|p_1 \times p_2\right\|^{-1/3}\sigma_1 + 1\right)$
Affine	$\varsigma = \left\|\alpha\right\|^{-1/2}\sigma$
Mixed Geometry restricted to $\beta_2 = 0$	$\varsigma = \frac{3}{traceA\beta_1} \ln\left(\frac{traceA\beta_1}{3c}\left\|p_1 \times p_2\right\|^{-\beta_1}\left\|\alpha\right\|^{-1/2\beta_0} z + 1\right)$
Mixed Geometry not restricted	$\varsigma = \frac{1}{\frac{1}{3}traceA\beta_1 + u\beta_2} \ln\left(\frac{\frac{1}{3}traceA\beta_1 + u\beta_2}{c}\left\|p_1 \times p_2\right\|^{-\beta_1}\left\|\alpha\right\|^{-1/2\beta_0} y_1^{-\beta_2} z + 1\right)$, only circular spirals

Table 2.1: $\alpha = \det A - \frac{2}{9}Trace^2(A)$, y_1 is related to the initial conditions, u is a real part of an eigenvalue of A and C is a constant which is determined by the individual contributions of the three geometries (see Bennequin et al. (2009)).

geometric approach of using osculating orbits has proved useful in previous studies (Olver et al. (1994), Calabi et al. (1998)). Yet, during this computational pursuit, we have discovered an important theoretical result about the mixed geometry and the minimum jerk models which is particularly resurfacing for affine orbits. It is possible to obtain a movement that is both in compliance with the minimum-jerk and the mixed geometry models, and furthermore that the full affine curvature of these trajectories is constant. The mixed geometry model provides a set of parameters with which a path can be traversed. Here is a schematic description of our solution. A parametrization is defined by a set of values β_2, β_1 and β_0 which represent constant tensorial weights of the Euclidean, equi-affine and affine geometries, respectively. In addition, those weights are subject to the convexity constraint $\beta_i \geq 0$, $\sum \beta_i = 1$, $1 \leq i \leq 3$. We separate our inspection according to the different families of affine orbits, namely, to conic sections, monomials, standard log-spiral and elliptic log-spirals. Surprisingly, for all (standard) log-spirals there exists a set $\{\beta_i\}$ such that the induced movement is a solution of the constrained minimum-jerk model. Depending on the rate-of-growth of the argument of the spiral, we selectively receive that either $\beta_0, \beta_1, \beta_2 \geq 0$ or that at least one weight is negative, $\beta_i < 0$. In other words, the log-spirals are divided to those for which there exist a mixed-geometry parameter (with $\beta_i \geq 0$) such that the resulting movement is a minimum-jerk movement, and to those for which the same holds except that the constraint $\beta_i \geq 0$ is violated. For monomials, which include parabolas and hyperbolas and generally affine transformation of the standard Cartesian Equation $Y = X^\alpha$ for some fixed α, we get that there exists a finite family $\{\alpha_i\}$ for which the minimum-jerk and the mixed geometry descriptions coincide. In any case, the relation between the tensorial mixture of the mixed geometry model and the minimum-jerk model is given analytically.

We now describe the analytic solution for the mixed-geometry - minimum-jerk mapping. First we show how to find a minimizing jerk mixed geometry parameter (z) for non-elliptic logarithmic spirals by assuming that $\beta_2 = 0$ (we assume absence of Euclidean geometry contribution). In fact,

we proved that there could not be any Euclidean contribution that minimizes jerk, for strictly elliptic logarithmic spirals.

Non-Elliptic Logarithmic spirals

Consider the orbit given by the full affine Lie algebra generator:

$$\begin{pmatrix} 1 & b \\ -b & 1 \end{pmatrix}$$

The jerk-minimizing mixed geometry set of parameters (defined by the betas) are expressed as a function of b as in the matrix above which is the inverse of the orbit rate-of-growth parameter by,

$$\begin{aligned} \beta_1 &= 117/160 + \frac{1}{160} 3^{1/2} Y + \frac{1}{160}(3858 + \\ &\quad 36000b^2 - 120X - 226800/Xb^2 - 8760/X \\ &- 963000/Xb^4 + 378000/Y3^{1/2}b^2 + 37422/Y3^{1/2})^{1/2} \end{aligned} \tag{2.2}$$

$$\begin{aligned} Y &= (643 + 6000b^2 + 40X + 75600/Xb^2 + 2920/X + 321000/Xb^4)^{1/2} \\ X &= (169245b^4 + 22275b^2 + 595 + 118125b^6 + 6(-158724750b^6 - \\ &\quad 5916900b^4 - 1838769600b^8 - 103005b^2 - 9032428125b^{10} - 972 - 139683750000b^{12})^{1/2})^{1/3} \end{aligned}$$

And vice-versa, the variable b defining the non-elliptic orbit can be expressed as a function of mixed geometry parameters (defined by betas)

$$\begin{aligned} b &= \pm 1/30(900 + 9000\beta_1\beta_2 + 3000\beta_1^2 + 6750\beta_2^2 \\ &- 3600\beta_1 - 5400\beta_2 \pm 10 \\ &\quad (6480 + 333720\beta_2^2 + 390825\beta_2^4 + 1042200\beta_1^2\beta_2^2 - 803520\beta_1^2 \\ &\quad \beta_2 - 1205280\beta_1\beta_2^2 + 463200 \\ &\quad \beta_1^3\beta_2 + 1042200\beta_1\beta_2^3 + 444960 \\ &\quad \beta_1\beta_2 + 148320\beta_1^2 - 178560\beta_1^3 - 602640 \\ &\quad \beta_2^3 + 77200\beta_1^4 - 51840\beta_1 - 77760\beta_2)^{1/2})^{1/2} \end{aligned} \tag{2.3}$$

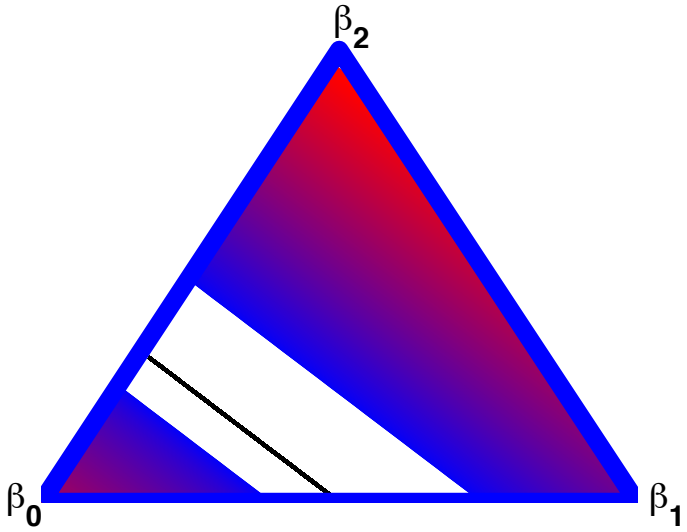

(a)

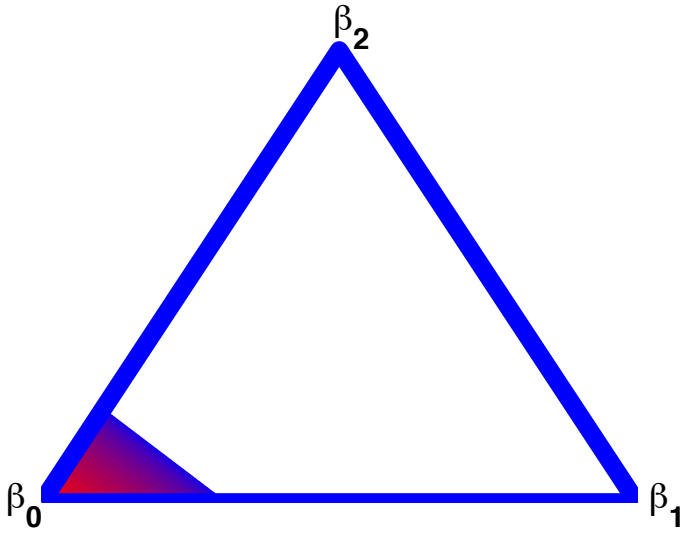

(b)

Figure 2.1: The minimum-jerk map of logarithmic spirals with respect to the mixed geometry parametrization. Color designates the spirals' parameter rate-of-growth (real part of the eigenvalue of generating matrix). For each spiral there is a straight line of appropriate β's of the form $\beta_1 = -\frac{2}{3}\beta_2 + \textit{constant}$ where the constant depends on the spiral's parameter. In (a) three different solutions are depicted: the black solution is independent with the spiral (and hence colored in a neutral color) the two other solutions and the solution in (b) are continuous in the rate-of-growth-parameter. Finally, the fifth solution lies outside of the mixed-parameter triangle.

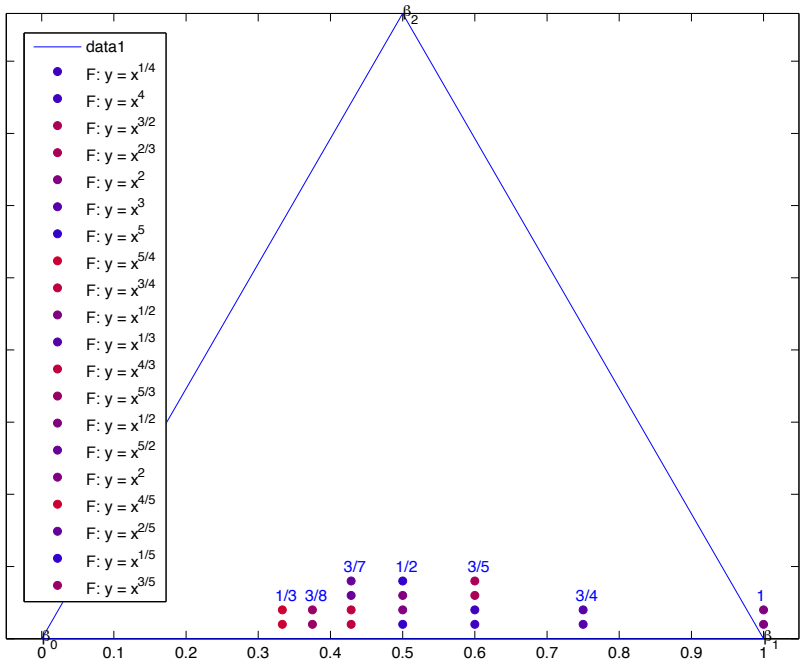

(a)

Figure 2.2: The minimum-jerk map of monomials with respect to the mixed geometry parametrization. For specific values of β_1 ($\beta_1 = 1/3, 3/8, 3/7, 1/2, 3/5, 3/4, 1$, $\beta_2 = 0$) there exist monomials for which the respective parametrization attains a minimum jerk solution. Importantly, these solutions are invariant under affine transformations - the respective mixed parametrization assumes a minimum-jerk for a given monomial indifferently to affine transformation

Monomials

Consider the monomial orbit for which the matrix A has the following form:

$$\begin{pmatrix} 1 & b \\ 0 & d \end{pmatrix}$$

Solutions for the jerk minimizing mixed geometry parameters impose that d in the matrix above satisfies $d^{\pm 1} \in \{4/5, 3/4, 2/5, 3/4, 1/5, 1/2, 1/4, 2/3, 1/3, 1\}$. These correspond, up to affine transformations, to the following free minimum jerk solutions (Flash and Hogan (1985)): $Y^n = X^m$, where $n, m = 1, 2, 3, 4, 5$. The mixed geometry parameters are given in the following table:

β_1:	$\frac{1}{3}$	$\frac{3}{8}$	$\frac{3}{7}$	$\frac{1}{2}$	$\frac{3}{5}$	$\frac{3}{4}$	1 (equi-affine or 2/3 power law)
d:	$\frac{4}{5}$	$\frac{3}{5}$	$\frac{2}{5}, \frac{3}{4}$	$\frac{1}{5}$, 2 (parabolas)	$\frac{1}{4}, \frac{2}{3}$	$\frac{1}{3}$	2 (parabolas)

Table 2.2: Monomials and their jerk-minimizing mixture of geometries ($\beta_2 = 0$).

Generalization of previous works

The intimate relations we have discovered between the mixed geometry and the minimum-jerk models were already partially addressed by previous works ((Polyakov et al. (2009a), Bright (2007))). Since the mixed geometry model was not established at that time, most of the theoretical consideration was confined to the connection between the equi-affine parametrization and the minimum-jerk model. Our analytic expressions revalidate and generalize Polyakov Polyakov (2001), Polyakov et al. (2009a) and Bright Bright (2007) results. Polyakov found that all parabolas can be traversed so that the equi-affine speed is constant, as well as a minimum-jerk parametrization is attained. Bright added another special spiral for which this property holds and further spirals for which Euclidean and full affine speed profiles are constant, all attaining a minimum-jerk parametrization for their respective paths. Since Euclidean, equi-affine and (full) affine parameterizations are special cases of the mixed geometry model, our results generalize all of these previous findings. We also prove that this agreement between the models does not hold for any of the non-planar full affine orbits.

Law of Motion	Minimum-Jerk Curves (affine orbits)
Euclidean (constant speed)	Straight lines, log spiral $b = \frac{1}{\sqrt{5}}$
Equi-Affine (2/3 power law)	Parabolas, log. spiral: $b = \frac{\sqrt{7}}{3}$
Affine (Isochrony)	Log spiral: $b = \frac{1}{\sqrt{5 \pm 2\sqrt{5}}}$
Mixed Geometry	Log spirals mapped by geometric mixtures $b = f_i(\beta_0, \beta_1, \beta_2) : i = 1, ..., 5$, All circular Log spirals conditioned by: $\beta_1 = \frac{1}{2} - \frac{3}{2}$

Table 2.3: $\begin{pmatrix} 1 & b \\ -b & 1 \end{pmatrix}$ is the generator of the orbits in the table. The five equations f_i that map mixed geometry parameterizations into minimum-jerk trajectories is complicated and hence left out of this report.

The equi-affine moving frame

We shall express the equi-affine moving frame in terms of the osculating conic to the curve and the Euclidean curvature at that point. First, as explained also by Bennequin et al. Bennequin et al.

(2009), using the method of Cartan moving frame, the equi-affine moving frame is expressed as:

$$\frac{dM}{d\sigma_1} = I_1, \tag{2.4}$$

$$\frac{dI_1}{d\sigma_1} = I_2, \tag{2.5}$$

$$\frac{dI_2}{d\sigma_1} = \kappa_1 I_1, \tag{2.6}$$

where κ_1 is the equi-affine curvature, σ_1 the equi-affine arclength, I_1 the equi-affine tangent and I_2 the equi-affine normal.

Let us demonstrate that the equi-affine moving frame can be found using geometric entities alone. The coefficients of the osculating conic are easily expressed in Cartesian coordinates using simple algebraic operations Calabi et al. (1998). It can be shown that the equi-affine normal lies in the direction of the aberrancy of a plane curve (see also in Schot (1979)). As elegantly shown by Schot, the aberrancy of a curve, which measures the asymmetry of a curve about its normal Schot (1978), is an affine invariant, thus its direction agrees with the equi-affine normal, I_2. Also, the axis of aberrancy of a curve at the point of interest coincides with the axis of aberrancy of the osculant conic, which is passing through the center of the conic for ellipses and hyperbolas and through the point at infinity for parabolas (i.e. the axis of the parabola which is perpendicular to the directrix of the parabola). Once the direction of I_2 is geometrically obtained from the osculant conic, its magnitude can be obtained using the radius of curvature. We develop the equi-affine frame in terms of the Euclidean arch-length, s, using the known relation between the equi-affine arclength and the Euclidean arclength Bennequin et al. (2009), $d\sigma_1 = \kappa^{\frac{1}{3}} ds$:

$$I_1 = \kappa^{-\frac{1}{3}} T, \tag{2.7}$$

$$I_2 = \kappa^{-\frac{5}{3}} \kappa_s T + \kappa^{\frac{1}{3}} N, \tag{2.8}$$

where T and N stand for the Euclidean tangent and normal, respectively, and k is the Euclidean curvature and s subscripts denote derivatives with respect to the Euclidean arclength parameter, s. The size of I_2 is now given a geometrical meaning:

$$|I_2| = \frac{\kappa^{\frac{1}{3}}}{\cos\alpha},$$

where α is the angle between the axis of aberrancy and the (Euclidean) normal. In addition, we get a nice geometric interpretation of the derivative of the Euclidean curvature with resect to Euclidean arclength,

$$\kappa_s = \kappa^2 \tan\alpha.$$

Finding the osculant affine orbit

The one item which is not geometric in our procedure is the calculation of the full affine curvature. As detailed in Bennequin et al. (2009), the full affine curvature can be calculated by differentiating the equi-affine curvature,

$$\kappa_0 = \frac{d}{d\sigma_1}\kappa_1^{-\frac{1}{2}}. \tag{2.9}$$

The full affine curvature, taken together with the previous items that were calculated geometrically, gives us a closed form expression of A, the generator of the orbit. In the Supplementary Materials Section, we develop in detail this analytic formulation calculated in terms of the point of osculation, the Euclidean tangent and equi-affine normal as well as the curvatures, κ_0, κ_1,κ_2.

Segmentation Based on Affine Osculant Primitives

The properties of affine orbits in terms of the minimum-jerk and the mixed geometry models make them natural candidates for subserving as building blocks of complex human trajectories. We propose a segmentation based on locally defined geometric properties as expressed by the full affine moving frame. A set of affine orbits was defined in relation to each of the points on a general curve and a measure of distance between those orbits and the curve was calculated (Figure 2.3(a)). An optimality criterion was used to pick subsets from those osculant segments that reliably represent the parameterized trajectories (Meirovitch (2008)). Figure 2.3(b) depicts an example of this segmentation for the original and an affinely transformed lemniscate.

The following description assumes a sampled trajectory, $r(n) \in \mathbb{R}^2$, $n = 1, ..., N$.

1. For each data point i
   (a) Calculate $\psi_i(\nu)$, the osculating affine orbit.
   (b) Find the maximal boundaries $\nu_1 < \nu_2$ such that

$$\text{Hausdorff}(\{\psi_i(\nu)\}_{\nu=\nu_1}^{\nu_2}, r(n)_{n=1}^{N}) < \epsilon_0$$

   (c) Project the boundaries $\psi_i(\nu_1)$ and $\psi_i(\nu_2)$ on data points $r(n_1), r(n_2)$.
   (d) Store $S_i = (n_1, n_2)$.
2. Use dynamic programming to choose a subset of $\{S_i\}_{i=1}^{N}$ that is temporally compatible (no overlaps of segments) while maximizing the number of samples in each S_i (Meirovitch (2008)).

Examining affine invariance, the osculating orbits to the transformed shape are the affine transformations of the osculating orbits to the original shape. Indeed, the result of segmenting the

affinely transformed lemniscate is the affine transformation of the segmentation of the original lemniscate, indicating the success of the numerical procedure, in spite of the fact that the trimming of the orbits based on a threshold corresponding to some Euclidean Hausdorff distance is not affinely invariant.

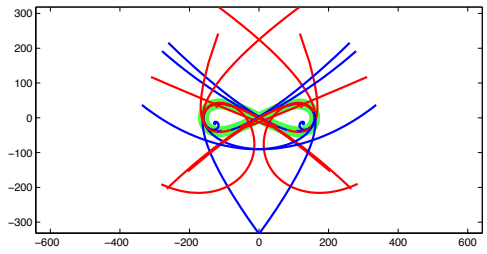

(a) Osculating orbits - Lemniscate.

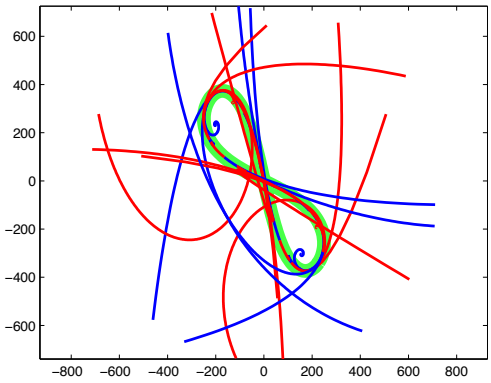

(b) Osculating orbits - affinely transformed Lemniscate.

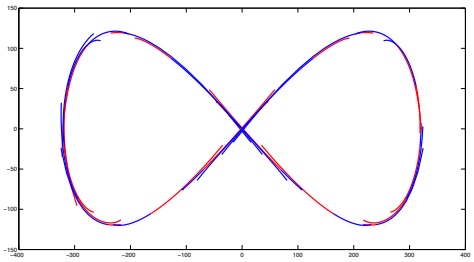

(c) Trimmed osculating orbits - Lemniscate.

Figure 2.3: In (a) and in (b), the osculating affine orbits were calculated for every tenth point on two Lemniscates, which are related to each other by an affine transformation. Each osculation point divided the osculating curve into two branches, referred to here as "left" and "right" branches and colored in blue and red, respectively. In (c), the osculating orbits were calculated and subsequently restricted using Hausdorff distance on a large scaled Lemniscate.

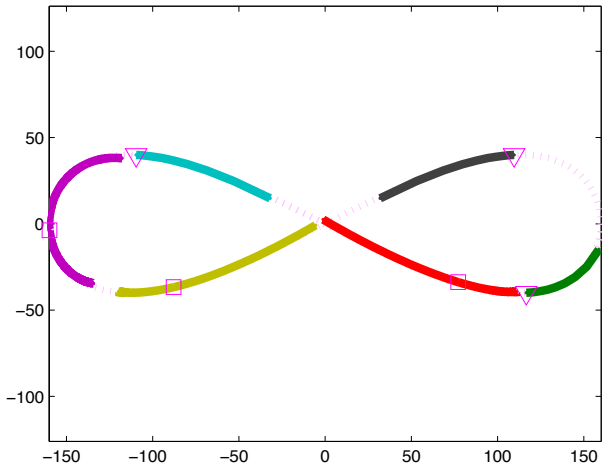

(a) Lemniscate.

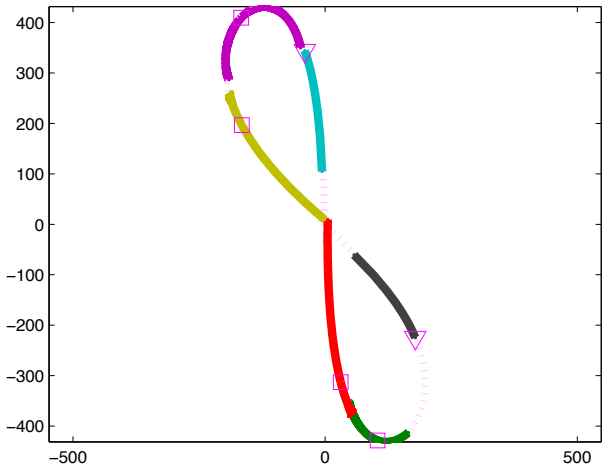

(b) Affinely transformed Lemniscate.

Figure 2.4: The optimal segmentation method in Meirovitch and Flash (2013) was adapted and used to select a subset of osculating segments, where for each osculation point three segments were generated according to "left", "right" and "left-right" branches of the osculating curve, where "left-right" included both the "eft" and "right" sides of the osculating orbit (see Figure 2.3). Graphical triangles, diamonds and squares mark the osculation points in correspondence to whether the selected segments was "left", "right" or "left-right", respectively. The similarity between the segmentations in (a) and (b) with respect to the geometry of the Lemniscates stems from the affine invariance of the osculating orbit. It should be noted that the trimming according to the Hausdorff distance is not an affine invariant, but still under the threshold of the algorithm the difference seems negligible. The colors of the segments are given for the sake of illustration.

Chapter 3

From geometric singularities to kinematic representation

The kinematics of human drawing and locomotion movement is well represented by the classical geometries (i.e Euclidean, equi-affine, affine, paper in prep. and Bennequin et al. (2009)). However one of the difficulties with fitting movements based on any specific non-Euclidean geometry is in the exceptional cases where one of the local geometries attains singularity. In this section we will define these singularities and show how to use them in order to constrain the kinematic representation. There are no singularities of the Euclidean geometry so in the following part we will focus on the geometrical singularities of the equi-affine and full affine geometries.

Equi-affine singularities

The equi-affine geometry (the geometry describing the 2/3 power law) is not suitable for movements whose curvature changes sign. These changes in direction occur at path-points, Ψ, called inflection points. The geometry in the neighborhood of an inflection point is special and admits the limit

$$\lim_{\psi \to \Psi} \kappa(\psi) = 0,$$

where κ is the Euclidean curvature of the path parameterized by ψ. This equation can be expressed in terms of Euclidean and equi-affine geometries. For the Euclidean and equi-affine arc-lengths, ds and $d\sigma$, respectively, one (equivalently) has

$$\lim_{\psi \to \Psi} \frac{d\sigma}{ds} = 0,$$

which simply means that the equi-affine arc-length vanishes faster than the Euclidean arc-length at inflection points. The last equation constrains the equi-affine speed which is readily observed when parameterizing the trajectory with time (marked by t),

$$\frac{\dot{\sigma}(\Psi)}{\dot{s}(\Psi)} = 0, \tag{3.1}$$

where $\dot{()}$ is the derivative with respect to time so that $\dot{\sigma}$ is the equi-affine speed and $\dot{s}$ is the Euclidean speed. It is thus impossible to travel through inflection points with non-zero constant equi-affine speed. In terms of the mixed geometry model this constraint translates to the mixing constraint $\beta_1 \neq 1$. However it is a-priori not clear whether other values $0 \leq \beta_1 < 1$ are possible. Interestingly, infection points can be traveled with a general mixture such that

$$\beta_1 = 3\beta_0. \tag{3.2}$$

This is known to be the only mixture that is valid for an arbitrary inflection point (Bennequin et al. (2009); and we found that specific inflection points can be constructed from affine orbits and be traveled with other mixtures).

Full affine singularities

The full affine geometry (which accounts for the isochrony principle) is not suitable for describing the kinematics along parabolic points which correspond to neighborhoods with vanishing points of the equi-affine curvature. A parabolic point admits the limit,

$$\lim_{\psi \to \Psi} \kappa_1(\psi) = 0,$$

where κ_1 is the equi-affine curvature. Analogously to the case above for equi-affine geometry, one has

$$\kappa^{\frac{1}{3}} \kappa_1^{\frac{1}{2}} = 0 \rightarrow \frac{d\sigma_1}{ds} = 0,$$

which means that the full-affine arc-length, σ_1, vanishes faster than the Euclidean arc-length, ds. In kinematic terms, this translates to

$$\frac{\dot{\sigma_1}(\Psi)}{\dot{s}(\Psi)} = 0,$$

which entails that a non-vanishing full affine speed is not possible (see the analogous calculation above for the equi-affine geometry). The equivalent mixing constraint of the mixed-geometry model

is that $\beta_0 \neq 1$. It appears that for parabolic points the only general mixing constraint is

$$\beta_0 = 0. \tag{3.3}$$

Reduced degrees of freedom

The idea that human movement is segmented according to the locations of inflection points was originally suggested in Lacquaniti et al. (1983) and was later developed as a segmentation criterion Viviani and Cenzato (1985) based on the breakdown of the 2/3 power law. This was however shown to be equally predicted by a constrained minimum jerk model (Todorov and Jordan (1998)) that does not explicitly represent any segmentation of the trajectory Richardson and Flash (2002). The mixed geometry model Bennequin et al. (2009) also suggests that inflection points are not necessarily breakdowns of a kinematic regularity (e.g. 2/3 power law). A segment, containing an inflection point, can be parameterized by a mixture of the type $\beta_1 = 3\beta_0$ (Equation 3.2), without breaking down the regularity. This representation, we suggest here, may constrain the kinematic degrees of freedom of an otherwise complex mixed geometry kinematic representation of a longer path. Moreover the following is a different intuition than the one developed in the case of discrete segments – an inflection point is a via-point in the kinematic representation and not a discrete point at which segments abruptly change. The same reasoning is equally applied to parabolic points with the mixing constraint $\beta_0 = 0$ (Equation 3.3).

The mixed geometry equations model the kinematics using three tensorial weights $\beta_i \geq 0$, such that $\sum \beta_i = 1$. As we have seen, geometric singularities add another constraint so that the total number of degrees of freedom per singularity is 1 – this is called here the Mixture Model Target at the Singularity (MTS).

Using $\{\alpha_k\}$-SIK) for representation

Human kinematics is known to be locally related to the geometric properties of the path (Bennequin et al. (2009)) however it is not clear how much information is required for the representation of the complex human kinematics. Here we examine whether assigning control variables to the singularities may be used for kinematic representation of the entire trajectory using interpolation of the beta weights.

The set of parameters $\{\alpha_k\}$-SIK) suggests a modulation in the kinematics along a path which is based on fixed control parameters at the singularities, which were called MTS. It is a-priori unknown whether there exist a set of parameters $\{\alpha_k\}$ such that the interpolated weight functions, $\beta_i(\psi)$, adequately represent the mapping from path to kinematics. To examine this, we formulate the task as a fitting problem by incorporating a cost function to be minimized. For simplicity the

cost function used is the average squared residual of the SIK speed profile and the parameter space is R^N whose coordinates are the $\{\alpha_k\}$ sets, where N is the number of singularity points.

Algorithm

The algorithm used is now described in a bullet style. Here $r(t)$ is a human trajectory.

1. Preprocess:

   - Fit the path traversed by $r(t)$ with an analytic function $\Omega(\psi)$ in the least squares sense, e.g. by a least-square decomposition over a set of Fourier basis functions (from the pseudo inverse). The choice of the basis functions may have effect on the performance of the algorithm. Here we used $n = 18$ for the cosine and sine components for each coordinate and a basic fundamental frequency which was optimized. Notes: (a) Care should be taken to avoid over-fitting. (b) For enhanced efficiency the total equi-affine archlength of $r(t)$ can be used for scaling the number of points whose error is considered.
   - Obtain $\Omega(t)$ by characterizing $\Omega(\psi)$ to comply with $r(t)$. The solution can be derived by a descent method since Ω is known everywhere. For our data it worked better to employ such an approach for a sunset of points and fill in the rest of the points using spline reparameterizations.
   - Calculate, $\kappa(t), \kappa_1(t)$ the geometric profiles of in the analytic representation Ω for the time parameter, t.
   - Obtain the singularity points Ψ_k and group according to the corresponding geometries (i.e., equi-affine full affine).

2. Minimize the expected error $E\left[\left(|\dot{r}(t)| - \hat{v}(t)\right)^2\right]$:

   - Consider a set of parameters $\{\alpha_k\}$.
   - Compute $\hat{\beta}_i(\Psi_k)$ according to Equation **??** and interpolate for t.
   - Compute $\hat{v}(t)$ based on the mixed geometry expression

$$\hat{v}(t) = \prod_i V_i(t)^{\hat{\beta}_i(t)}$$

The evaluation of the predicted mixed profile can be done from the geometric profiles by (Bennequin et al. (2009)):

$$\hat{v}(t) = C\kappa(t)^{-\frac{1}{3}(\beta_1(t)+\beta_0(t))}\kappa_1(t)^{-\beta_0(t)}$$

.

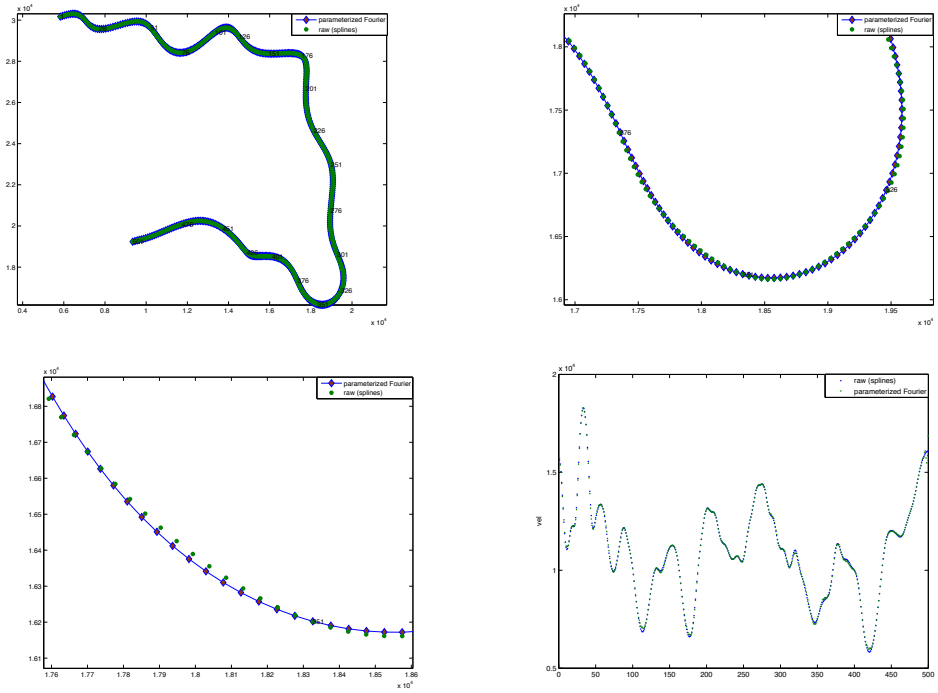

Figure 3.1: Scribing example. The first three panels correspond to different resolutions. The shape of the raw data is well represented by the path Fourier curve (16 harmonics of a basic frequency with X two phases X 2 coordinates). Raw data were projected on the analytic curve using non linear regression for each data point (panel (c)). The representation of the kinematics is a critical issue in this work; panel (d) shows that the velocity profile of the raw data is accurately projected on the Fourier curve.

Results

The algorithm is currently tested in an ongoing study of human locomotion. We now demonstrate the accuracy of the different steps of the algorithm on several examples of drawing movements.

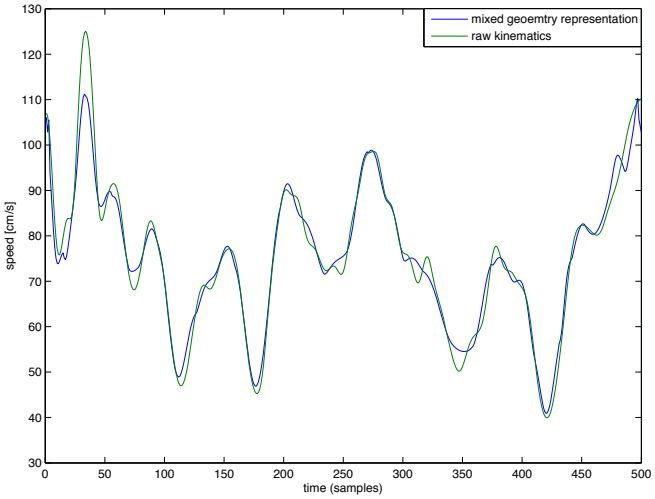

(a) Geometry-induced and human speed profiles

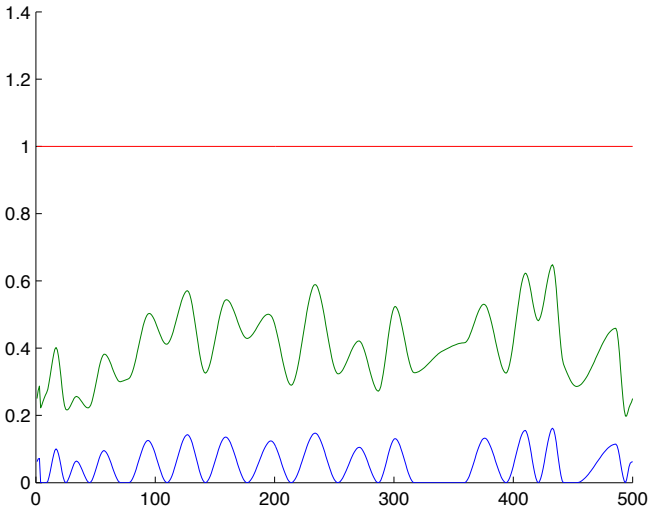

(b) Representation by beta profiles

Figure 3.2: The kinematic representation of a the scribing example (Figure 3. The kinematics are quite well represented by the geometry of the path while the beta parameters are optimized at the singularities according to the SIK representation described in the text.

Chapter 4

The geometrical redundancy in the mixed geometry model

In Bennequin et al. (2009) the human drawings of several shapes (see Viviani and Flash (1995)) were compared against the kinematic predictions of the mixed geometry model. It was shown that the humans path were segmented according to the kinematic fit given by the three coefficient weights, β_0, β_1 and β_2, as described in the Introduction and in Bennequin et al. (2009). Those beta weights were plotted for each of the shapes (cloverleaf, limacon and lemniscate) and modality (drawing, walking) across all trials subjects.

Here we reexamined the origins of the variability in these data, assessing whether the model itself exhibits statistical redundancies in the model's parameter space. To this end, we discovered that for the cloverleaf there exists a linear relation between the β_0 and β_1 such that the velocity profiles defined by each of the respective beta weights are statistically indistinguishable ($R^2 > 0.98$), as depicted in Figure 4.1(a).

The redundancy map appearing in the upper left panel was calculated using the following patching algorithm. The parameter space was quantized in obtaining a discrete set of possible beta values that represent distinct, statistically distinguishable speed profiles. The speed profile corresponding to $\beta_1 = 1$ was calculated (equi-affine parametrization, or the 2/3rd power law), which is referred to as the representative profile of the first equivalence group of parameters. Then all beta weights whose speed profiles are statistically indistinguishable from this representative profile are marked as belonging to the first group. A representative for the next equivalence group is chosen as the one giving the best agreement, in terms of R^2, with the previous representative. The process is iterated until all beta weights are examined. Each of the groups for an analytic cloverleaf were plotted as in Figure 4.1(a) where the colors designate the beta weights using an RGB scheme for triplets $[\beta_0, \beta_1, \beta_2]$.

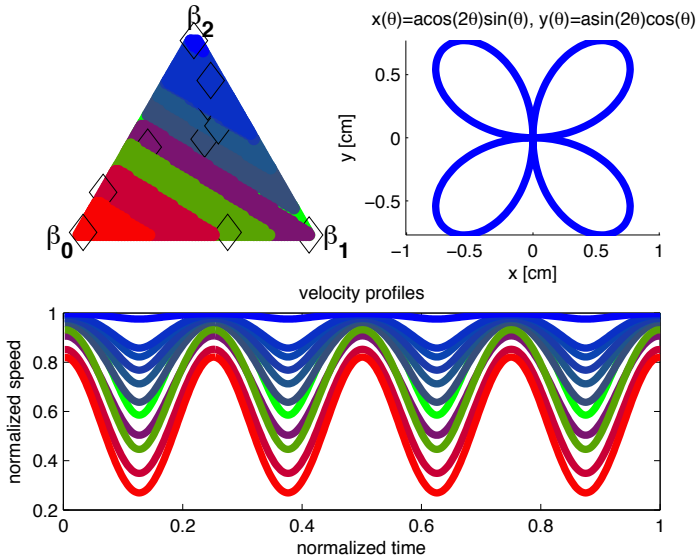

(a) The velocity profiles were calculated for the analytic cloverleaf. The top-right panel depicts the shape of the cloverleaf. The mixed geometry triangle in the top-left panel is colored according to the statistical equivalence of parametrizations of the cloverleaf. The bottom panel depicts the different speed profiles that match the different groups of speed profiles (see the text for more information)

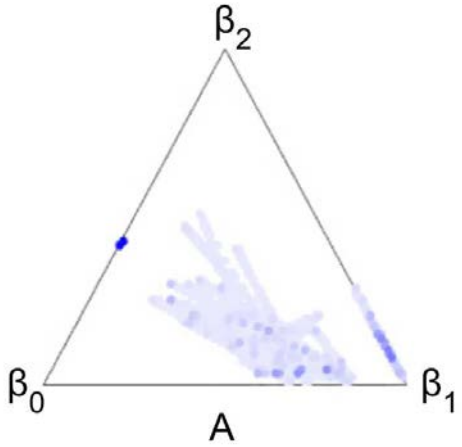

(b) The trajectories were adopted from Bennequin et al. (2009). The points in the triangle designate the mixed geometry parametrization for the cloverleaf across subjects.

Figure 4.1: The variance of the data presented in the bottom panel is mostly explained by one equivalence group in the top panel, which suggests that the different segments in the human data employed mixed geometry wights that are statistically indistinguishable. See the text for a detailed description.

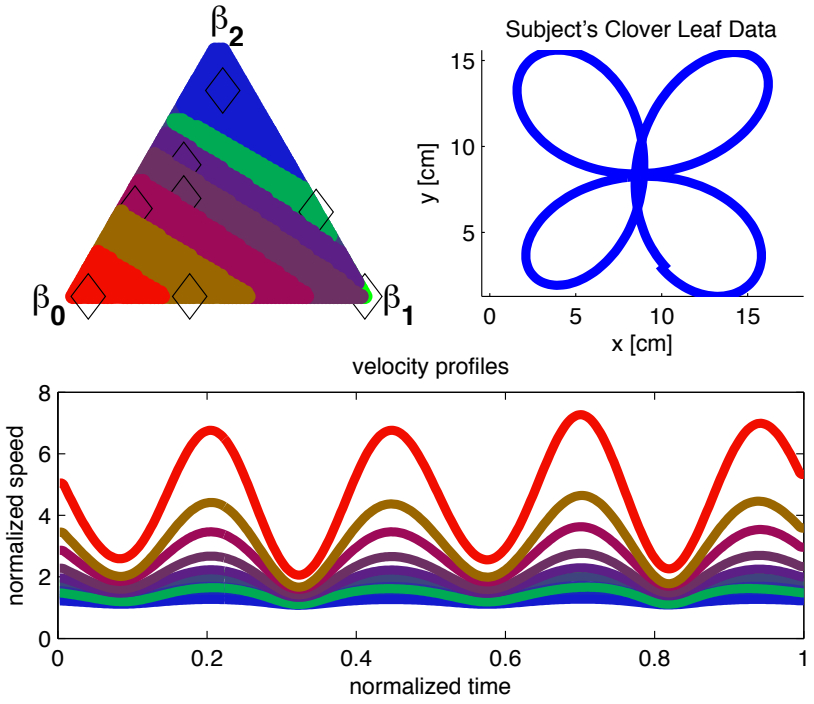

Figure 4.2: The analysis described in Figure 4.1 was carried out for an example if subject trajectory adopted from Bennequin et al. (2009). The patter appearing in the analytic example of cloverleaf in Figure 4.1 applies also for the subject data.

The distribution of beta values appearing in Bennequin et al. (2009) for the drawing of the cloverleaf (Figure 4.1(b)) can be explained by the redundancy map (Figure 4.1(a)). We suggest here that the control procedure must be invariant with respect to the profiles belonging to the same equivalence class. In particular, the profiles represented in Figure 4.1(b) are similar from a motor control point of view. This suggests that the humans may select a straight line in the parameters space rather than a unique point.

To check the last claim on real data, the groups of speed profiles were calculated for the analytic cloverleaf that was used as stimulus in Bennequin et al. (2009) (Figure 4.1(a)) and for the subject's actual speed profiles in Figure (4.1(b) were calculated using regression on the real paths produced by the subjects. To elucidate whether the redundancy is well apparent in real data, the above statistical grouping was further carried out on a real trajectory from Bennequin et al. (2009). The same statistical tendency was seen also in the real data, as shown by Figure 4.2. An example of another shape adopted from Bennequin et al. (2009), the limacon, is depicted in Figure 4.3(a).

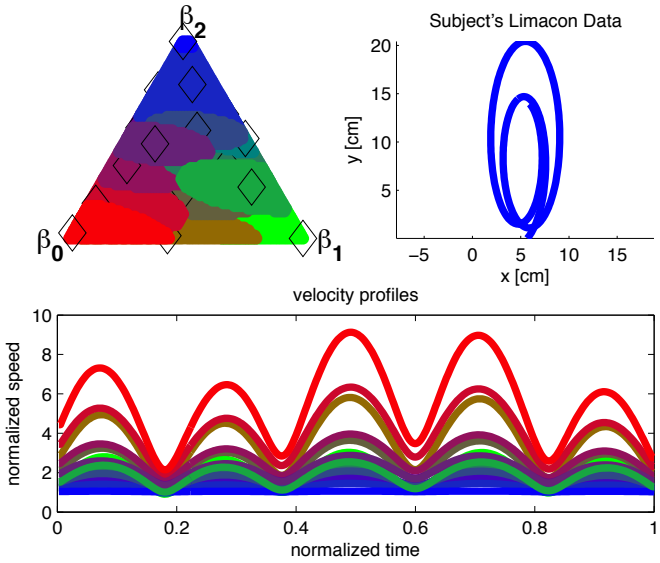

(a) The velocity profiles were calculated for the analytic limacon. The top-right panel depicts the shape of the limacon. The mixed geometry triangle in the top-left panel is colored according to the statistical equivalence of parametrizations of the limacon. The bottom panel depicts the different speed profiles that match the different groups of speed profiles (see the text for more information)

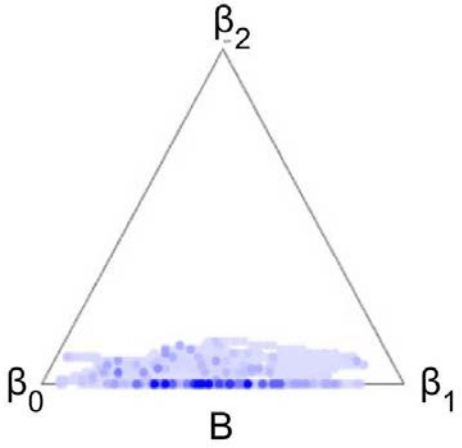

(b) The trajectories were adopted from Bennequin et al. (2009). The points in the triangle designate the mixed geometry parametrization for the limacon across subjects.

Figure 4.3: Most of the variance in the fitted beta weights (lower panel) is explained by one equivalence class (top panel). The mixed geometry segments that were found in the cloverleaf movements (Bennequin et al. (2009)) correspond to beta wights that predict statistically indistinguishable kinematic profiles. See the text for a detailed description.

Chapter 5

Segmenting sign language into motor primitives with Bayesian binning

The endpoint trajectories of sign language movements fulfill characteristic power laws linking velocity and curvature Meirovitch (2008), Meirovitch and Flash (2013). The parameters of these power laws typically vary between different segments of longer action sequences. These parameters might thus be exploited for the unsupervised segmentation of signs into movement primitives. We investigated whether such segments can be identified by Bayesian binning Endres and Földiák (2005), using a Gaussian observation model whose mean has polynomial time dependence. We showed that this method yields reasonable segmentation and correctly models individual segments of ground-truth data. Importantly, polynomial orders between 3 and 5 defined models with optimal trade-off between complexity and accuracy of the trajectory approximation, in accordance with general principles from motor control, the minimum jerk model and the minimum acceleration model.

"Ground Truth" Segmentation

Our main goal was to examine whether the Bayesian binning (BB) approach may subserve the segmentation of natural movements into segments that are consistent with the known power law kinematic regularity that was shown to organize various kinds of human movement and sign language movements in particular Meirovitch and Flash (2013). To achieve this objective, the raw data were reparameterized to adhere with the power laws along segments whose boundaries, from

a motor control point of view, were arbitrarily chosen. From a computational point of view, we used regularity criteria to ascertain that biologically implausible segmentations were left out of the analysis based on the smoothness of the data near the segmentation points, the compliance with the power law and the degree of agreement with the timing of the subjects segments. In practice, we randomly picked a segmentation, assigned beta values for each of the segments, and discarded those segmentations that violated one of those regularity requirements. The main pitfall in our methodology is that our ground truth segmentation does not yield motion primitives and thus the resulting consistency with the BB is particularly an agreement between the kinematic regularities of the power laws and the polynomial observation model. To better examine the question of agreement with motion primitives, the organization of power law segment, as appearing in the raw data, should be used instead of the arbitrary decomposition. The problem in applying the BB on real trajectories, without following a "ground truth" synthesis, is that decomposition into primitives, and particularly power law segmentation, is still an open question in motor control research. For example, it is widely accepted that primitives generally co-articulate in time in forming complex movements Meirovitch and Flash (2013) which as well include time transitions in between segmented kinematic regularities. This complexity also applies to the case of motor segmentation in terms of power laws (Meirovitch and Flash (2013)). This co-articulatory compliance with respect to power laws is demonstrated in Figure 5 for one sign language trajectory; the blue colors in the figure mark good compliance and the red colors mark poor compliance. It is readily seen that, although power laws imply on a discrete organization of the motor articulation, there is still no unique and obvious way to define the resulting segmentation. As our objective is to examine the possible contribution of BB to motor control questions, the analysis must rely on computationally well posed motor segmentations. The compliance with the power laws for a trajectory with synthesized kinematics is shown in Figure 5. It is readily seen that there is less ambiguity about the possible power law segmentation of the trajectory. In effect, comparing to Figure 5, it is rather straight forward to automatically identify those right-angle vertices of the blue triangles in Figure 5, which designate the synthesized segments. The full details of the study are described in a separate manuscript (submitted).

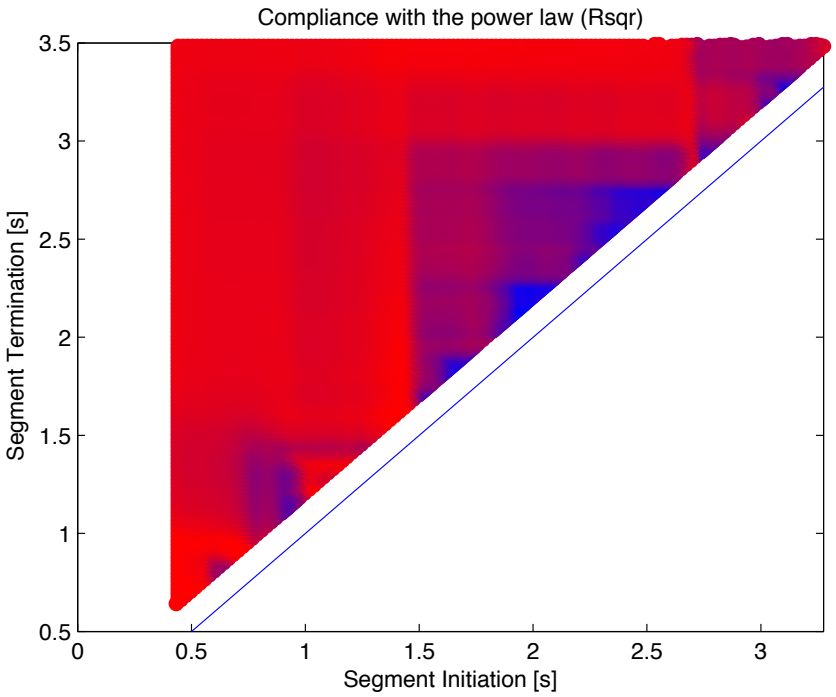

Figure 5.1: The compliance with the power law is demonstrated for a sign language trajectory adopted from Meirovitch (2008). Each point in the graph designates a trajectory segment where blue colors designate high compliance with the power law and red colors degradation of the law. It is readily seen that although power laws imply on a discrete organization of the motor articulation, there is still no unique and obvious way to define the resulting segmentation.

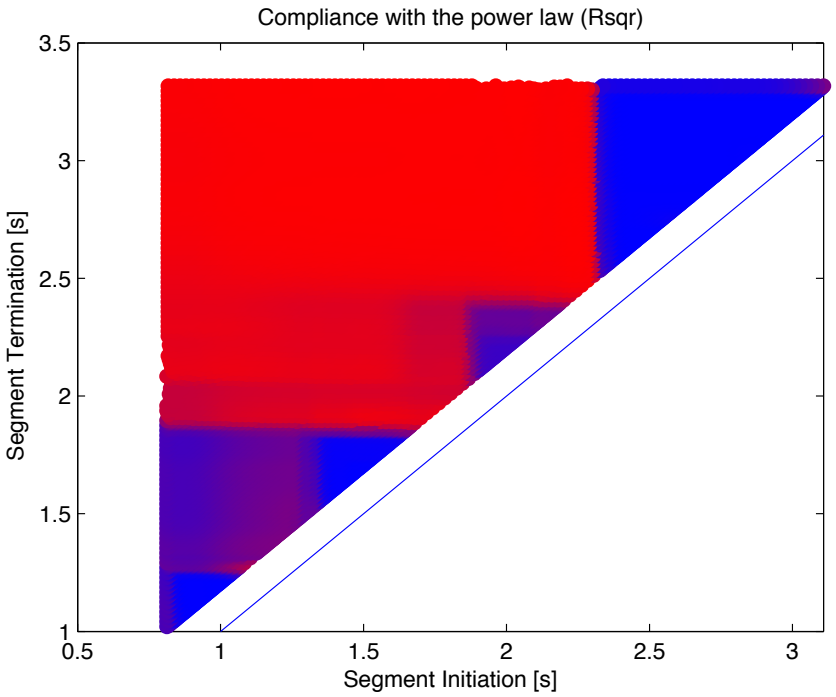

Figure 5.2: The compliance with the power laws is shown for a trajectory with synthesized kinematics. Each point in the graph designates a trajectory segment where blue colors designate high compliance with the power law and red colors degradation of the law. It it readily seen that there is less ambiguity as to do with the possible segmentation of the trajectory in comparison to the real subject trajectory (see Figure 5). In effect, comparing to Figure 5, it is rather straight forward to automatically identify those right-angle vertices of the blue triangles in Figure 5, which designate the synthesized segments.

Chapter 6

Discussion

In this deliverable we presented a new theory for motion primitives based on the composition of the classical Euclidean, equi-affine and full affine geometries. The shapes of these primitives are governed by the orbits of 1-parameter subgroups acting on fixed points in task space. Examples of such orbits are straight lines and circles (Euclidean geometry), parabolas, ellipses and hyperbolas (equi-affine geometry), elliptic logarithmic spirals and monomials (full affine geometry).

Representation of geometry

Representing complex movements based on such geometrical primitives is plausible for several reasons.

First, from a theoretical point of view, the geometrical simplicity of orbits makes them attractive candidates for serving as primitives because they generalize the symmetry of points, straight lines and circles to other non-Euclidean geometries which were studied before in computer vision research (Calabi et al. (1998); Olver et al. (1994)). The orbits map among themselves by specific transformations for each individual geometry. Moreover, any two points on a parabola can be mapped one upon the other, and the parabolas can map on other parabolas, by equi-affine transformations.

Second, among these orbits some were already suggested as movement primitives in motor control research. For example parabolas were extensively studied before (Polyakov et al. (2009b), Handzel and Flash (1999)). It was shown that parabolas are geodesics of equi-affine geometry (Guggenheimer (1977)) and that moving at a constant equi-affine speed along parabolas (i.e., obeying the 2/3 power law) automatically minimizes the jerk of the movement (Polyakov et al. (2009a)) and that any parabola can be obtained from one parabolic prototype by applying affine transformations.

The third reason to use orbits is related to invariance and optimal kinematics. We developed the

differential geometry tools needed for representing the geometry-dependent kinematics along orbits (Euclidean, equi-affine and full affine) and discovered that the natural kinematic rules of a specific geometry, namely moving at a constant speed under that geometry, along several affine orbits coincides with the predictions of the constrained minimum jerk. Moreover, the mixed geometry model (Bennequin et al. (2009)) and the constrained minimum jerk model (Todorov and Jordan (1998)) are mutually obeyed for a large family of affine orbits. For each circular logarithmic spiral there exists a special mixture of Euclidean, equi-affine and full-affine geometries (called mixed parameter) that minimizes the jerk along that orbit, suggesting that invariance and smoothness are closely related motor concepts. The invariance of the affine orbits under all affine transformations suggests that along orbits representation of the movement and its segmentation are especially compact. A movement can be represented independently of the choice of Cartesian frame because all full affine invariants do not depend on any choice of a global frame used for representation - a movement can be automatically recognized from different points of view (even when it follows non Euclidean yet affine transformations).

To allow representation of complex tasks we offered the notion of using the orbit primitives as building blocks which can be temporally concatenated. However we do not approximate the observed behavioral movements based on the best fitting primitive but rather use as candidate for segmentation only the orbits that (locally) osculate with points along the orbits in task space behavioral trajectories. This new approach for segmentation enables to find segmentations of complex movements that are invariant to affine transformations and not only having a primitive that is invariant. The reason is that best fitting primitives will not remain optimal following affine transformations while the affine differential properties defining the osculating orbit are unaffected by any such manipulation.

Representation of kinematics

We later moved on to the representation of the behavioral kinematics based on mixing geometrical rules of the classical geometries (Bennequin et al. (2009)). It is a-priori not clear whether the curvature profiles can predict the kinematics of a complex movement and what variables are required for a successful representation. Here we suggest that very little information should be modulated at the extremal points of the equi-affine and full affine geometries, called geometric singularities. Based on several theorems developed in Bennequin et al. (2009) we suggest that one parameter per singularity point should be assigned and can be used in determining the mixture of geometries and that the weights of the three geometries governing the movement in between singularities are constructed by interpolation of these weights. For now we examined these kinematic representations in drawing movements and started to work also with data from locomotion. In an ongoing work we attempt to determine the mixture of geometries at the singularity points based on the overall

smoothness along the complex movement.

This idea of reducing the number of parameters needed for kinematic representation (here 1 per singularity) was also implemented for a constant mixture of geometries. In Bennequin et al. (2009) it was found that human trajectories tend to use specific mixtures of geometries that tend to be linearly related. We found out that these mixtures are in fact statistically related and that their kinematic predictions are quite similar, especially for highly symmetric shapes such as the cloverleaf. In fact this linear relationship in the space of mixture of geometrical rules resurfaces in several different studies: one of the jerk-minimizing solutions over circular affine orbits is admitted by a family of mixtures of geometrical rules that are linearly related to each other (in the beta space), the mixtures that enable movements along inflection singularities and those through parabolic singularities are also linearly related and finally both human movement and the statistical properties of the model suggest redundant representations of the mixing of different geometries that are special to the case of symmetrical paths. Taken together this meeting point of theoretical and behavioral findings suggests that optimal mixtures are met by linear relations among the weights used for the different geometries and that the laws of movement derived from the mixed geometries model are simpler than previously thought.

Extracting differential invariants from highly complex motor tasks

Finally, in the last section (Endres et al. (2013)) we went further to implement the ideas discussed here (and in the literature, see Viviani and Flash (1995); Richardson and Flash (2002)), suggesting that differential invariants and optimization are related principles in highly complex movements and that these may be applicable even in the case of noisy end-effector recordings. We recorded the wrist movements of two Israeli Sign Language (ISL) users and time warped their kinematics so that they perfectly adhere to, segment-wise, generalized power laws. To maintain biological realism we made sure that unreliable kinematics were not analyzed and that the durations of movement in each segment were the same in the real data and in the time-warping. We discovered that Bayesian Binning (BB), using a Gaussian observation model whose mean has polynomial time dependence, may uncover the power law underlying segmentation. We therefore revalidate and extend previous findings that showed convergence between the 2/3 power law and the minimum jerk models because the BB model partitions the data according to the most probable polynomial segmentation optimizing for the degree of polynomial needed for segmentation.

Bibliography

Abend, W., Bizzi, E., and Morasso, P. (1982). Human arm trajectory formation. *Exp Brain Res*, 105:331–348.

Bennequin, D., Fuchs, R., Berthoz, A., and Flash, T. (2009). Movement timing and invariance arise from several geometries. *PLoS computational biology*, 5(7):e1000426.

Bernstein, N. (1967). *The Co-ordination and Regulation of Movements*. Pergamon Press, Oxford.

Bizzi, E., Tresch, M., Saltiel, P., and d Avella, A. (2000). New perspectives on spinal motor systems. *Nature Reviews Neuroscience*, 1(2):101–108.

Bright, I. (2007). Motion planning through optimization. Master's thesis, Weizmann Institute of Science.

Calabi, E., Olver, P., Shakiban, C., Tannenbaum, A., and Haker, S. (1998). Differential and numerically invariant signature curves applied to object recognition. *International Journal of Computer Vision*, 26(2):107–135.

Endres, D. and Földiák, P. (2005). Bayesian bin distribution inference and mutual information. *IEEE Transactions on Information Theory*, 51(11).

Endres, D., Oram, M., Schindelin, J., and Foldiak, P. (2008). Bayesian binning beats approximate alternatives: estimating peri-stimulus time histograms. *Advances in Neural Information Processing Systems 20*.

Endres, D. M., Meirovitch, Y., Flash, T., and Giese, M. A. (Submitted (2013)). Segmenting sign language into motor primitives with bayesian binning. *Frontiers in Computational Neuroscience*.

Faugeras, O. and Keriven, R. (1996). On projective plane curve evolution. *LECTURE NOTES IN CONTROL AND INFORMATION SCIENCES*, pages 66–73.

Flash, T. (1983). Organizing principles underlying the formation of hand trajectories. *Doctoral dissertation, Massachusetts Institute of Technology, Cambridge, MA*.

Flash, T. and Hochner, B. (2005). Motor primitives in vertebrates and invertebrates. *Current Opinion in Neurobiology*, 15(6):660 – 666. Motor sytems / Neurobiology of behaviour.

Flash, T. and Hogan, N. (1985). The coordination of arm movements - an experimentally confirmed mathematical-model. *J Neurosci*, 5(7):1688–1703.

Guggenheimer, H. W. (1977). *Differential Geometry*. Dover Publications.

Handzel, A., A. and Flash, T. (1996). Affine differential geometry analysis of human arm trajectories. *Abstracts of The Society for Neuroscience*, 22.

Handzel, A., A. and Flash, T. (1999). Geometric methods in the study of human motor control. *Cognitive Studies*, 6(3):309–321.

Harris, C. M. and Wolpert, D. M. (1998). Signal-dependent noise determines motor planning. *Nature*, 394:780–784.

Lacquaniti, F., Terzuolo, C., and Viviani, P. (1983). The law relating kinematic and figural aspects of drawing movements. *Acta Psychologica*, 54:115–130.

Lashley, K. (1951). The problem of serial order in psychology. *Cerebral mechanisms in behavior. New York: Wiley*.

Meirovitch, Y. (2008). *Kinematic Analysis of Israeli Sign Language*. Master thesis, The Weizmann Institute.

Meirovitch, Y. and Flash, T. (2013). Motor decomposition by power laws in israeli sign language. *Paper in preperation*.

Mussa-Ivaladi FA, B. E. (2000). Motor learning through the combination of primitives. *Philosophical Transactions of the Royal Society of London Series B-Biological Sciences*, 355:1755–1759.

Olver, P., Sapiro, G., Tannenbaum, A., et al. (1994). Differential invariant signatures and flows in computer vision: A symmetry group approach. *Geometry driven diffusion in computer vision*.

Pollick, Frank, E. and Sapiro, G. (1996). Constant affine velocity predicts the 1/3 power law pf planar motion perception and generation. *Short Communication*, 37(3):347–353.

Polyakov, F. (2001). *Analysis of monkey scribbles during learning in the framework of models of planar hand motion*. PhD thesis, The Weizmann Institute of Science.

Polyakov, F., Drori, R., Ben-Shaul, Y., Abeles, M., and Flash, T. (2009a). A Compact Representation of Drawing Movements with Sequences of Parabolic Primitives.

Polyakov, F., Stark, E., Drori, R., Abeles, M., and Flash, T. (2009b). Parabolic movement primitives and cortical states: merging optimality with geometric invariance. *Biological Cybernetics*, 100(2):159–184.

Richardson, Magnus, J. E. and Flash, T. (2002). Comparing smooth arm movements with the two-thirds power law and the related segmented-control hypothesis. *The Journal of Neuroscience*, 22(18):8201–8211.

Schot, S. H. (1978). Aberrancy: Geometry of the third derivative. *Math Mag*, (51):259–275.

Schot, S. H. (1979). Geometrical properties of the penosculating conics of a plane curve,. *The American Mathematical Monthly*, (4):449–457.

Todorov, E. and Jordan, M. I. (1998). Smoothness maximization along a predefined path accurately predicts the speed profiles of complex arm movements. *J. Neurophysiol*, 80:696–714.

Viviani, P. and Cenzato, M. (1985). Segmentation and coupling in complex movements. *Journal Experimental Psychology Humam Perception and Performence*, 11(6):828–845.

Viviani, P. and Flash, T. (1995). Minimum-jerk, two-thirds power law, and isochrony: Converging approaches to movementnext term planning. *J Exp Psychol Hum Percept Perform*, 21(1):32–53.

Viviani, P. and McCollum, G. (1983). The relation between linear extent and velocity in drawing movements. *Neuroscience*, 10(1):211–218.